Journal of Physics and Chemistry of Solids 202 (2025) 112686

Contents lists available at ScienceDirect

Journal of Physics and Chemistry of Solids

journal homepage: www.elsevier.com/locate/jpcs

Co-sputtering deposition of HfO_2 thin films: Insights into Cu and Ag doping effects

Abdullah Akkaya [a,*], Osman Kahveci [b], Sedanur Güler [c], Enise Ayyıldız [b]

[a] Mucur Technical Vocational Schools, Tech. Prog. Department, Kırşehir Ahi Evran University, Kırşehir, 40500, Turkey
[b] Department of Physics, Faculty of Sciences, Erciyes University, Kayseri, 38280, Turkey
[c] Graduate School of Natural and Applied Sciences, Physics, Erciyes University, Kayseri, 38280, Turkey

ARTICLE INFO

Keywords:
HfO_2 doping
Co-sputtering
XPS
TLM
Potentiodynamic polarization analyses

ABSTRACT

This study comprehensively examines the structural, electrical, and electrochemical properties of Cu- and Ag-doped HfO_2 thin films deposited via the co-sputtering method. The dopant concentrations were precisely controlled by varying the DC magnetron sputtering power, allowing a systematic evaluation of their impact on film characteristics. Structural analysis revealed that the monoclinic phase of HfO_2 was retained, with minor crystallographic changes attributable to the dopants. Also, confirmed the successful incorporation of dopant ions, revealing variations in spin-orbital splitting values due to differences in ionic radii and electronic configurations. Morphological studies demonstrated that Ag doping reduced surface roughness and enhanced uniformity, whereas Cu doping increased roughness, resulting in a more irregular morphology.

TLM analysis highlighted improved conductivity in doped films, although the effect was limited by the oxidation states of dopants and the presence of oxygen vacancies. Electrochemical investigations through potentiodynamic polarization analysis revealed that Ag doping significantly improved corrosion resistance in alkaline environments, while Cu doping had the opposite effect, reducing corrosion resistance due to increased porosity and morphological irregularities. The results underscore the contrasting roles of Cu and Ag doping in modulating the functional properties of HfO_2 thin films, offering insights into their potential for applications in advanced electronic devices, resistive switching memory, and energy storage systems.

1. Introduction

Hafnium dioxide (HfO_2), with its wide bandgap, high dielectric constant, and thermal stability, has emerged as a critical material in electronic and optoelectronic devices [1–3]. These unique properties make it an ideal candidate for various applications, piquing the curiosity of researchers and scientists [4,5]. The high dielectric constant of HfO_2 makes it suitable for replacing classical low-k materials in electrostatic capacitors, gate dielectrics in metal-oxide-semiconductor field-effect transistors (MOSFETs) and thin film transistors (TFTs), and other microelectronic devices, inspiring further exploration into its unique properties [2,6]. HfO_2 also exhibits excellent optical properties, such as high optical transmissivity and low reflectivity in the visible and near-infrared regions, making it ideal for antireflection optical coatings [3,7]. As a ferroelectric material due to its remanent polarization properties, it is a promising candidate for applications in memory devices, sensors and energy storage systems [3,8,9]. HfO_2, with its attractive structural properties, has been explored for its potential as a solid-state electrolyte in lithium-ion batteries. Its ionic conductivity offers the promise of higher energy density and improved safety conditions compared to conventional liquid electrolytes, making it a promising prospect for future energy storage systems [10–12].

In general, thin film growth techniques, deposition conditions and post-deposition treatments of HfO_2 films are highly effective on all structural parameters and chemical properties of the films. Therefore, HfO_2 films have been grown by many methods such as sputtering, physical vapor deposition (PVD), atomic layer deposition (ALD), pulsed laser deposition (PLD) and sol-gel etc. to control thin film parameters [13–21]. Also, post-deposition treatments such as annealing were applied to improve the HfO_2 films parameters [15–18]. The advantages and limitations of each method allow the deposition of films with the desired properties. Therefore, appropriate methods are selected for depositing films with properties suitable for the intended use. For example, ALD, PLD and sol-gel are preferred for the deposition of very

* Corresponding author.
E-mail address: abdullah.akkaya@ahievran.edu.tr (A. Akkaya).

https://doi.org/10.1016/j.jpcs.2025.112686
Received 6 January 2025; Received in revised form 4 March 2025; Accepted 7 March 2025
Available online 13 March 2025

thin and high-quality HfO_2 films, sputtering technique has gained considerable attention due to its potential advantages such as scalability and high deposition yields [6,20–23]. Sputtering is an effective deposition technique for growing high-purity films and has advantages such as good adhesion, controllable thickness, elemental composition, and uniformity [3,13,20]. In addition, sputtering variables (e.g., background pressure, sputtering power, etc.) can be used to create precise growth conditions for the desired application [20].

In recent years, extensive research has focused on doping HfO_2 with various metals, such as Ni, Ta, Y, Nd, Si, Al, Gd, Ce, W, and Pt, to enhance its properties and expand its applications [6,18,22–27]. Among these, doping materials with semi-noble metals like copper (Cu) and silver (Ag) have garnered significant attention owing to their unique electrical and electrochemical characteristics [8,21,28–30]. These unique properties are a source of curiosity and a driving force for further research [29–32]. Doping HfO_2 with transition metals can modify its microstructure, phase composition, and electrical properties, potentially enhancing its performance in various applications. This enhancement potential highlights promising advancements for future HfO_2-based devices [18,23,33–35]. Improved electrical conductivity, dielectric properties, and structural properties are critical for applications in resistive switching memory devices, nonvolatile memory devices, and capacitors. These properties also affect the reliability and endurance of HfO_2-based devices, making them valuable for optimizing device performance [8,18,36]. In addition, doping has been shown to influence the electrochemical behavior of films, potentially enhancing their corrosion resistance and catalytic activity [27].

This study investigates the structural, electrical, and electrochemical properties of Cu- and Ag-doped HfO_2 thin films synthesized via co-sputtering. The dopant concentrations were controlled by varying the DC magnetron sputtering power, and the resulting films were characterized using a range of techniques, including X-ray diffraction (XRD), X-ray photoelectron spectroscopy (XPS), and scanning electron microscopy (SEM). Cu- and Ag-doped HfO_2 films were systematically fabricated and thoroughly characterized.

2. Materials and methods

2.1. Materials and synthesis

Cu- and Ag-doped HfO_2 films were grown by RF and DC magnetron sputtering onto boron-doped and thermally oxidized Si wafers. The oxide layer was 285 nm thick and provided good electrical insulation against the conductive substrate. Before deposition, the thermally oxidized p-silicon substrates were cleaned using standard RCA cleaning (i.e., a 10 min boil in $NH_4OH + H_2O_2 + 6H_2O$ followed by a 10 min boil in $HCl + H_2O_2 + 6H_2O$ and rinsed by deionized water and dried with high-purity nitrogen) [37]. Substrates were then dipped in 10 % HF solution, rinsed in deionized water, and dried under nitrogen flow. Subsequently, the substrates were immediately placed in the NVTS-400 deposition chamber (Fig. 1), and 30-nm high-purity gold was evaporated on the Si substrate. This Au layer was used as the back contact of the working electrode in order to minimize the effects of the Si substrate during electrochemical measurements.

Copper-bonded and 2-inch-diameter HfO_2 sputtering targets (99.95 %, Kurt J. The Lesker Company) for RF sputtering and Cu (99.99 %, Kurt J. Lesker Company) and Ag (99.995 %, Kurt. The Lesker Company) was positioned in the DC sputtering gun order. The growth process of the doped HfO_2 films was carried out in a 5 N high-purity argon flow (flow rate was 4 sscm). The constant RF power (for HfO_2 targets), substrate temperature, background pressure and substrate-cathode distance were 100 W, 30 °C, 8 mTorr, and 21 cm, respectively. The RF and DC sputter targets were arranged horizontally 25 cm apart, and both guns faced the substrate at a certain angle (~50°). The DC magnetron sputtering powers of the Cu and Ag dopants were 5, 10, and 20 W, respectively. The film thickness was monitored using a quartz crystal microbalance (QCM) thickness monitoring system and was fixed at 300 nm using an auto-shutter system. The continuous rotation speed of sample holder was 10 rpm for all deposition process.

TLM patterns were created using thermally evaporated high-purity gold contacts in a steel shadow mask. Data management for the SMU (Keithley, B2912A), and all calculations were conducted using the VEE Pro-based SeCLaS software [38,39].

2.2. Characterization

Field-emission scanning electron microscopy (FE-SEM) (Zeiss Gemini 500) was used to observe surface morphology and obtain information on the film's chemical composition. Mappings and X-ray energy-dispersive spectroscopy (EDS) results were analyzed using the FE-SEM Energy-Dispersive Spectroscopy software (FE-SEM-EDS) (EDAX Inc.). Atomic force microscopy (AFM-VeeCo Multimode 8) was used in

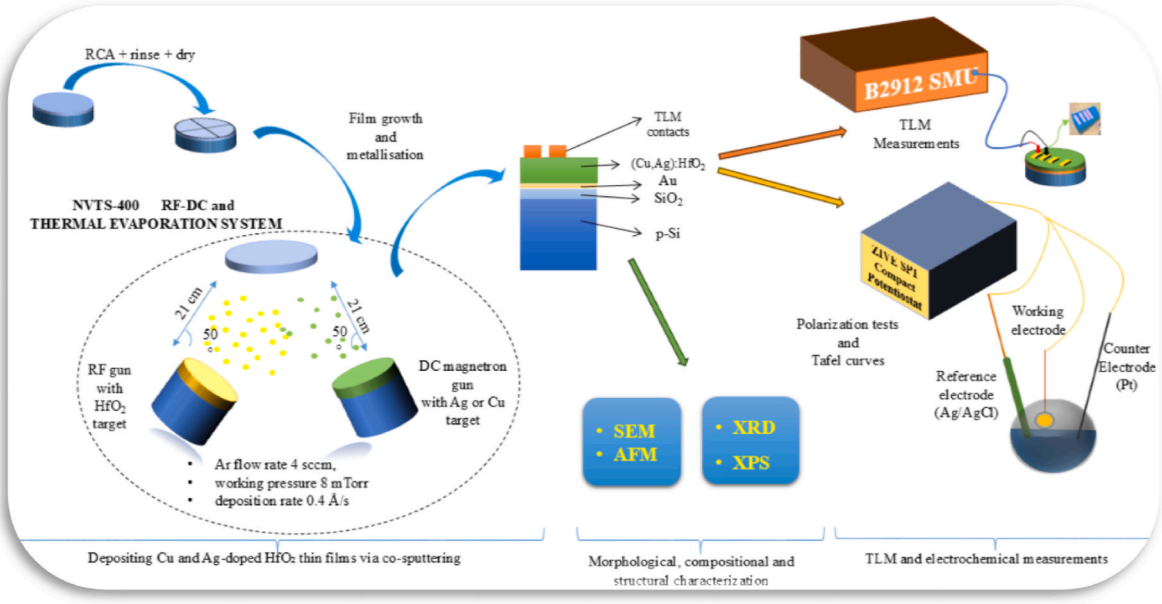

Fig. 1. Schematic illustration of the experimental setup for deposition and electrical and electrochemical measurements of Ag- or Cu-doped HfO_2 thin films.

tapping mode, during at 10 × 10 μm and 1 × 1 μm scan areas. 2D and 3D AFM images were recorded and mean surface roughness parameters were determined by using the NanoScope 3D Analysis software.

X-ray diffraction (XRD) patterns were recorded by a Pan Analytical Inc. X-ray diffraction (XRD) unit with (45 keV, 40 mA) in the scan range from 10° to 90° (2θ) and scan rate of 2°/min using Cu Kα radiation (λ = 1.5406 Å) as an X-ray source. Specs-FlexMod recorded X-ray photoelectron spectroscopy (XPS) measurements. Before survey scans of (Ag or Cu) doped HfO_2 films, they were slightly etched with Ar ions to minimize the effect of contamination on their surface. An XPS spectrometer was operated at 15 kV and the Al Kα radiation (with energy of 1486.7 eV). The Hf 4*f*, O 1*s*, Cu 2*p*, and Ag 3*d* plots were obtained by taking the average spectra of five scans for each element and using Gaussian–Lorentzian line shapes for deconvolution of the spectra.

The transfer length method (TLM) was used to determine the DC resistivity and contact properties. Current-voltage measurements (I–V) were conducted via a computer-controlled Agilent B2912A SMU. All measurements and calculations were performed using the VEE Pro-based SeCLaS software [38,39]. Potentiodynamic polarization tests of Cu- or Ag-doped HfO_2 thin films were conducted using a ZIVE SP1 Compact Potentiostat. The counter electrode was platinum wire, and the reference electrode was an Ag/AgCl (3 M NaCl) electrode. The working electrode probe was connected and immersed in a 0.1 M KOH electrolyte solution. Polarization tests were performed between a potential range of ±0.4 V and a scan rate of 1 mV/s.

3. Results and discussion

3.1. Morphological properties

3.1.1. FE-SEM-EDS characterization

Fig. 2a and 2b–d shows an FE-SEM image of the pure HfO_2 and Ag-doped HfO_2 thin films, respectively. As can be seen, Ag doping was observed to significantly change the surface morphology. The presence of Ag contributed to shaping the film's structure. Fig. 2c–e shows the FE-SEM images of the Cu-doped HfO_2 thin films. In this image, the Cu contribution caused noticeable morphological changes. So, Cu addition resulted in a more irregular and cracked structure. As a result, we observed that the Ag and Cu additives have different effects on the surface morphology of HfO_2 thin films. While the Ag additive improves the surface morphology and smoother structure, the Cu additive created an irregular and more brittle structure.

Further investigation of the distribution of doping atoms over the entire film is essential for depositing homogeneous films. The EDS mapping results for undoped and Ag- or Cu-doped HfO_2 thin films were homogeneous (Fig. 3). These data are essential for understanding the variation in the composition of thin films at different doping levels.

Table 1 presents the weights and atomic percentages of Ag and Cu in HfO_2 thin films doped at various power levels, as obtained by energy-dispersive spectroscopy (FE-SEM-EDS). The weights and atomic percentages of both elements were given at different power levels (5 W, 10 W, 20 W).

Atomic percentages values of Ag and Cu doped HfO_2 films indicate that co-sputtering was successfully applied to HfO_2 films. The weight percentage change caused by the increase in the sputtering power of the targets was more noticeable for Cu than for Ag. The atomic percentage of the dopants was determined from the EDS results and was 2.81 ± 0.51 % and 4.60 ± 1.73 % for Ag and Cu, respectively.

The weight percentage of Ag increased 15.38 ± 2.18 % to 16.52 ± 1.97 % with increasing sputtering power (5 W–20 W). Similarly, the Ag atomic percentage slightly increased from 2.81 ± 0.51 % to 2.96 ± 0.43 %. Despite the increased Ag targets' DC sputtering power, the atomic percentage increase remains limited. Similarly, the weight percentage of Cu increased from 9.32 ± 1.68 % to 16.92 ± 0.30 %, and the atomic percentage increased from 4.60 ± 1.73 % to 5.88 ± 0.15 % with increasing sputtering power. This shows that Cu sputtering seems more sensitive to sputtering power. Cu atoms are more integrated into the HfO_2 structure during doping due to their cluster formation tendencies, mean free path lengths of sputtered particles, sputtering yields, etc. [40,41].

3.1.2. AFM characterization

Surface morphology is an essential criterion for device applications because it can affect the electrical properties of thin films, especially when dielectric films used as interlayer smoothness can provide uniform contacts for electrical conductivity and prevent undesirable phenomena such as leakage current. Thus, the surface morphology of the metal-doped HfO_2 thin films should be as smooth as possible. The AFM images of undoped and Ag- or Cu-doped HfO_2 thin films were smooth without indistinguishable features (Fig. 4). The average surface roughness (Sa) and ten-point height (Sz) values of the grown materials were related to the differences in the surface structure. The surface roughness parameters of Ag- or Cu-doped HfO_2 thin films are presented as functions of the DC sputtering power (Table 2). The root mean square (RMS) roughness values and morphological structure of deposited films were remarkably similar to those reported in the literature [18,23,42–44].

As shown in Table 2, the root mean square (RMS) roughness value and the Sz value for undoped HfO_2 films are relatively low and indicate the Frank-van der Merwe (layer-by-layer) type growth mechanism [45]. However, the RMS and Sz values for HfO_2: Ag (5 W) thin films are quite

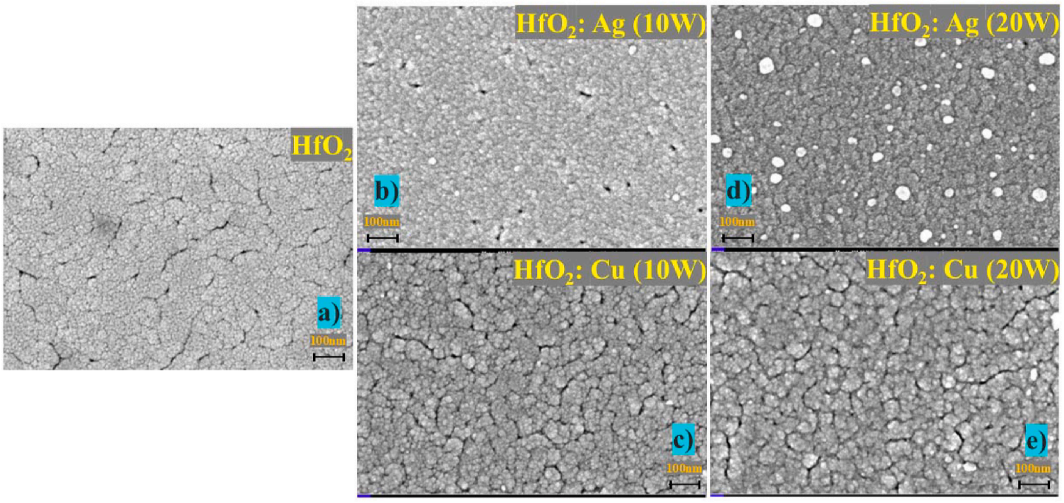

Fig. 2. For different DC sputtering power values, FE-SEM images of un-doped (a), Ag-doped (b,d), and Cu-doped HfO_2 (c,e) thin films.

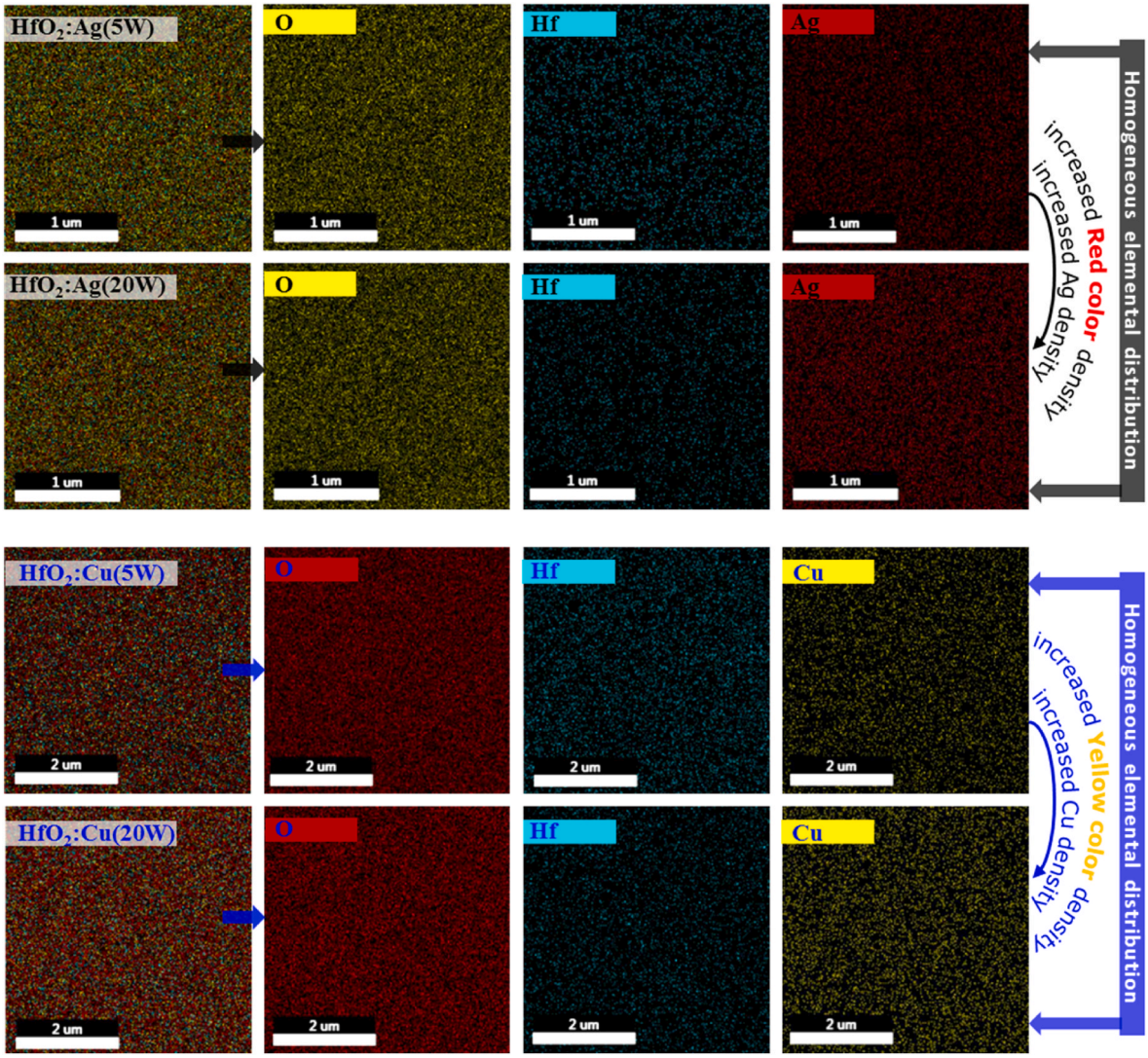

Fig. 3. EDS results for un-doped, Ag-doped, and Cu-doped HfO_2 thin films for different DC sputtering power values.

Table 1
Measured weighted and atomic percentages of simultaneously (Ag or Cu) doped HfO_2 films at various power levels by EDS.

Dc sputtering power	Ag-doped HfO_2		Cu-doped HfO_2	
	Weight %	Atomic %	Weight %	Atomic %
5 W	15.38 ± 2.18	2.81 ± 0.51	9.32 ± 1.68	4.60 ± 1.73
10 W	16.09 ± 1.94	2.88 ± 0.43	15.12 ± 1.97	5.65 ± 0.91
20 W	16.52 ± 1.97	2.96 ± 0.43	16.92 ± 0.30	5.88 ± 0.15

high. This indicates island (Volmer-Weber) type growth considering the growth method and film parameters (e.g. relatively thick films and sputtering method) [41,46,47]. As the Ag doping increased (at 5 W and 10 W), the surface roughness increases and island growth was the dominant mechanism. However, the roughness decreases at HfO_2: Ag (20 W). In fact, the change in surface energy caused by increasing Ag content indicates a return to a uniform structure (layer and island type). Similarly, at low Cu doping (at 5 W–10 W), the surface remains relatively smooth. However, when the sputtering power is increased (20 W) the roughness increases significantly, indicating that island type growth is dominant [20,48]. Furthermore, unintentional collisions (secondary collisions) in the sputtering chamber due to the more energetic particles traveling from the target toward the substrate may contribute to the change in these growth mechanisms [49,50].

3.2. Structural properties

3.2.1. XRD measurements

XRD characterizations were conducted to investigate the crystal structure of Ag- or Cu-co-doped HfO_2 thin films. Fig. 5a and b shows the XRD patterns recorded as a function of the HfO_2 films at different doping conditions. The XRD patterns of undoped HfO_2 and HfO_2:Ag (5 W) thin films showed a broadened diffraction peak around 31.8°. As seen in Fig. 5a–b, a few peaks of crystalline phases are observed in undoped HfO_2 and HfO_2:Ag (5 W) thin films. In this case, the film is not entirely amorphous and is a mixture of amorphous and crystalline phases with a small amount of crystals. The crystallite size of particles was determined using Debye–Scherrer's formula, and it was found to be 12 Å (for $2\Theta = 31.8°$) [20,25,51,52]. In this situation, crystallite size was close to the typical value for sputtered particles, indicating that HfO_2 was deposited on the substrate in a granular form [18,53].

Furthermore, the increase in doping resulted in an increase in crystallinity and this phase became the dominant phase with a small crystalline structure instead of remaining amorphous. Depending on the growth conditions, HfO_2 can exhibit several polymorphs, such as monoclinic (m-), orthorhombic (o-) and tetragonal (t-) phases [18,54,55]. So, peaks at $2\theta = 50.2°$ and 54.9° are assigned to *t*-(022) (JCPDS

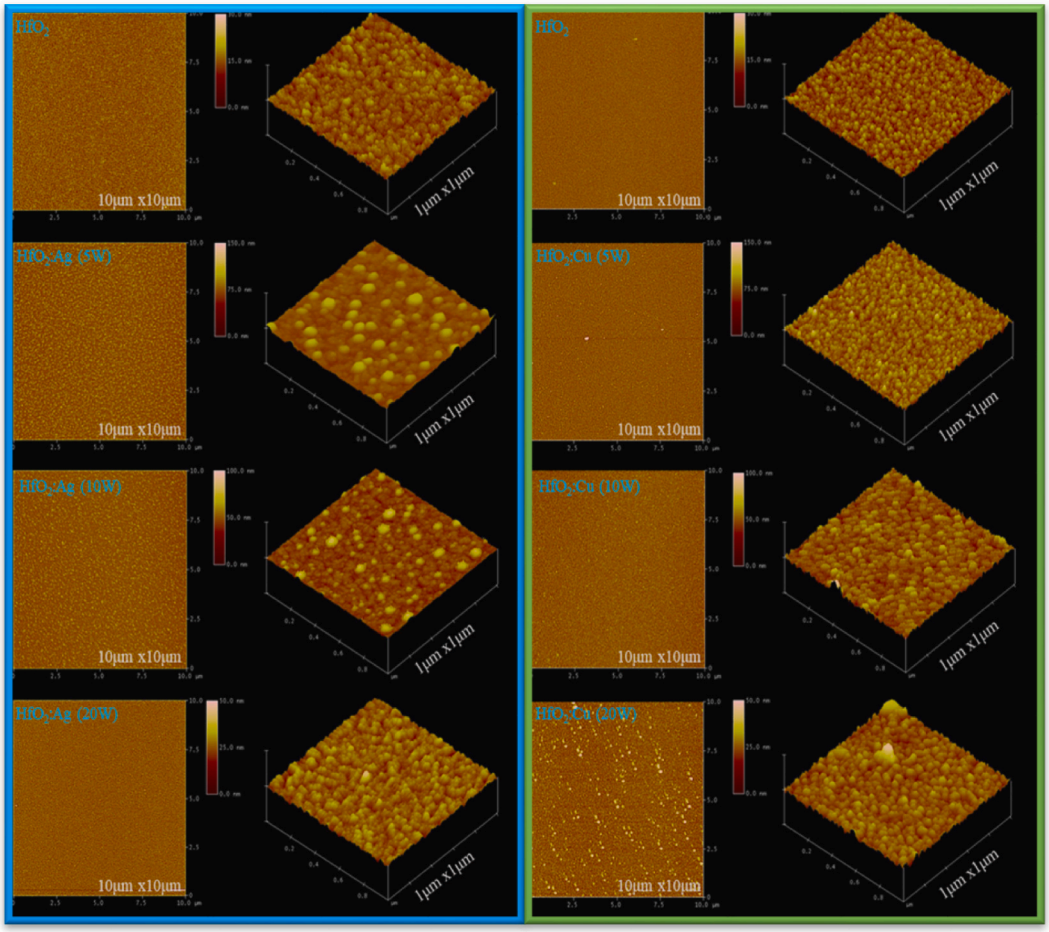

Fig. 4. 2D and 3D AFM images of un-doped, Ag-doped HfO_2 (left side) and Cu-doped HfO_2 (right side) films over a scan area of 10 × 10 μm and 1 × 1 μm.

Table 2
Surface parameter measurement results for simultaneously doped HfO_2 films.

DC sputtering power	Ag-doped HfO_2			Cu-doped HfO_2		
	RMS (nm)	Sa (nm)	Sz (nm)	RMS (nm)	Sa (nm)	Sz (nm)
–	2.45 ± 0.53	1.84 ± 0.41	8.14 ± 2.04	2.12 ± 0.43	1.58 ± 0.37	7.31 ± 1.45
5 W	7.41 ± 1.32	5.35 ± 0.89	24.94 ± 9.27	3.21 ± 1.17	2.32 ± 0.89	10.65 ± 3.85
10 W	5.99 ± 0.98	4.25 ± 0.84	19.99 ± 5.44	2.68 ± 0.68	2.01 ± 0.55	9.03 ± 2.62
20 W	2.92 ± 1.17	2.10 ± 0.80	10.15 ± 3.85	4.77 ± 1.60	3.38 ± 1.07	17.47 ± 7.96

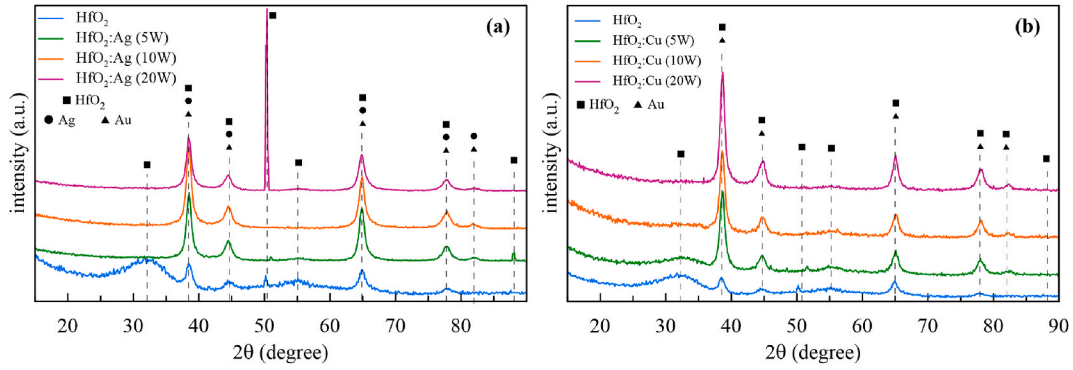

Fig. 5. XRD patterns of Ag- and Cu-doped HfO_2 thin films for different DC sputtering power values.

card no. 00-043–1017) and *m*-(202) (JCPDS card no. 00-08–342) of HfO_2, respectively [52,54–56]. These peaks may indicate the existence of a crystalline fraction and a mixture of monoclinic and tetragonal phases in the amorphous film [18,22,52,57,58].

Peaks from the Au layer just below the HfO_2 layer also exist in the spectrum, and these peaks are more clearly observed in Ag- or Cu-doped films (Fig. 5a). The peaks at 38.5°, 44.6°, 64.8°, 77.6°, and 82.0° also belong to Au (JCPDS card no. 00-002-1095), *c*-(111), *c*-(200), *c*-(220), *c*-(311), and *c*-(322) and mixed with the HfO_2 peaks, respectively. Fig. 5b shows that peaks related to metallic or oxide compounds of Cu could not be observed directly. Also, similar to the Ag-doped film's XRD results, diffraction patterns from the Au layer just below the HfO_2 layer exist here, too.

The diffraction patterns of Ag (JCPDS card no. 00-004-0783) and Au are similar, so we cannot interpret definitively whether Ag is crystalline or amorphous from our data. However, Cu was amorphous and probably sputtered Ag under similar conditions. The presence of this amorphous phase can be explained by the effects of parameters such as sputtering power and background pressure [59]. In other words, smaller grains and structures with more vacancies appear when the sputtering power is low, and the background pressure is high. Moreover, as observed here, high deposition pressures lead to a phenomenon known as the self-shadowing effect [59,60]. This effect causes atoms to impact at oblique angles instead of reaching the surface at a straight angle, leading to distortion of the crystal structure and a lower crystal quality. Furthermore, low sputtering power and high background pressure cause atoms to have reduced energy when reaching the surface, reducing their ability to diffuse at the surface. As a result, atoms arrive at the surface with insufficient energy, leading to a disordered arrangement that prevents the growth of an ordered crystalline structure.

3.2.2. *XPS measurements*

The XPS survey spectra show characteristic peaks for HfO_2:Ag and HfO_2:Cu thin films. Figs. 6 and 7 show the XPS survey spectra of HfO_2: Ag and HfO_2: Cu thin films. These spectra were recorded in the spectral range of 0–1400°eV after etching the surfaces of the films with Ar^+ to remove surface contaminants. The elemental analysis of the samples showed a series of characteristic peaks of Hf, O, and dopant atoms (Ag, Cu) and Auger peaks of O and dopant atoms (Ag, Cu). However, no substrate peak was observed, and a weak C*1s* peak was attributed to surface contamination, indicating incomplete Ar^+ sputtering.

The collected core-level elemental spectra of the Hf 4*f* peaks were fitted to two peaks at 16.61 and 18.20 eV, which correspond to the spin-orbital splitting of Hf $4f_{7/2}$ and Hf $4f_{5/2}$, respectively (Fig. 8.). The Hf $4f_{7/2}$ and Hf $4f_{5/2}$ peaks were separated by 1.6 eV each other, which

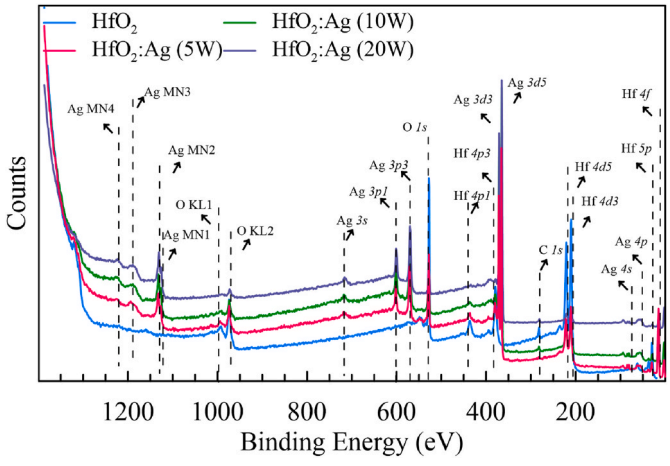

Fig. 6. Survey XPS spectra of the un-doped and HfO_2: Ag thin films. The spectra also show Auger peaks for Ag (MN1-4) and O (KL1-2).

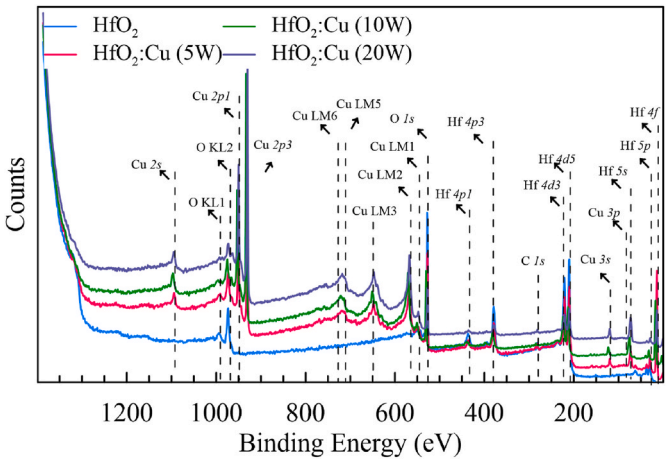

Fig. 7. Survey XPS spectra of un-doped and HfO_2: Cu thin films. The spectra also show Auger peaks for Cu (LM 1–5) and O (KL 1–2).

confirms that Hf is present as Hf^{4+} and Hf–O bonding exists [35,61–63]. When silver was introduced to HfO_2 films, the spin-orbital splitting value slightly increased to 1.7 eV and remained constant for all doping powers. However, Cu doping did not change the spin-orbital splitting value, remaining almost constant (~1.61 eV) for all HfO_2: Cu samples (Fig. 9).

This phenomenon can be explained by the different ionic radii of the dopant atoms [61,64]. Spin-orbit splitting results from an electron's spin interaction with the magnetic moment generated by the electron's orbital motion. Therefore, a change in the electric or magnetic field affecting the electrons in the valence band causes polarization effects and local electric field changes, resulting in a change in the value of spin-orbit splitting energy. Here, the Ag^+ ion has a larger ionic radius and a higher electron density than the Cu^{+1} ion. Therefore, it can lead to more significant polarization effects and changes in the local electric field. Moreover, Cu atoms with smaller ionic radii are likely to have a more limited interaction with the outer orbital electrons of Hf atoms, and their effect on the spin-orbital splitting value is too limited to be observed. The ionic/covalent character of oxides has a great influence on the electronic structure and properties of materials [65,66]. When two oxides are mixed, the cation of the more ionic metal oxide is expected to become even more ionic after the formation of the complex oxide due to charge transfer [66]. Due to the significant amounts of cations (Ag and Cu), doping causes the charge of Hf to be lost, and the Hf 4*f* peak shifts to a higher binding energy.

The binding energies (BEs) of core-level electrons are significantly affected by the chemical environment of atoms, a phenomenon often referred to as chemical shift, and its quantification allows the identification of bond structure and its variations [67]. Thus, the binding energy shift is usually associated with many structural factors, such as charge transfer, charge density distribution, and hybridization [18,64,68]. The charge transfer effect is regarded as the dominant mechanism causing this shift.

Fig. 10 shows the deconvoluted core-level peaks of HfO_2: Ag thin films for different DC sputter powers. As can be seen, the spin-orbital splitting energy was constant for all DC sputtering powers of the dopant atoms, and the peak positions of Hf 4*f* slightly changed (Fig. 10 a). This change may have originated from Ag doping into the film, which caused by a change in the oxidation states of Hf [18,66,69]. Fig. 10 (b) show deconvoluted O 1*s* spectra of HfO_2: Ag thin films. The deconvoluted peaks have two parts, and the binding energies correspond to lattice oxygen (O $1s_A$) and non-lattice oxygen (O $1s_B$) [18]. The calculated area ratio (at. %) of the O 1*s* peaks and non-lattice oxygen ratio increased with increasing Ag doping ratio (Table 3). This increment was related to oxidation of Ag dopant atoms and formation of Hf's suboxide.

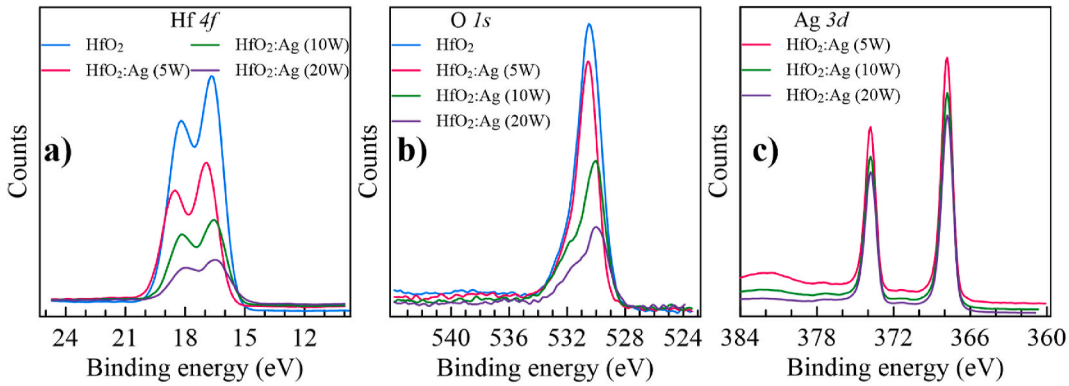

Fig. 8. Core-level XPS spectra of the Hf 4*f* (a), O 1*s* (b) and Ag 3*d* (c)regions of HfO_2: Ag thin films for different DC sputter power.

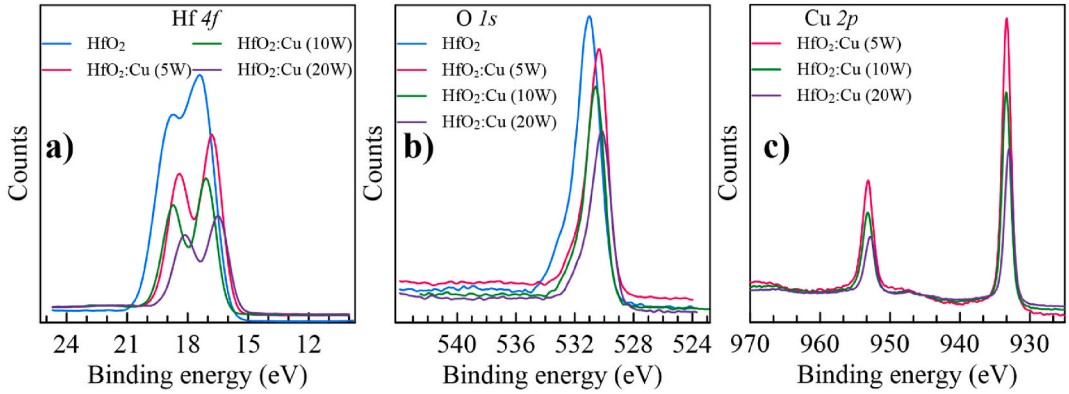

Fig. 9. Core-level XPS spectra of the Hf 4*f* (a), O 1*s* (b) and Cu 2*p* (c) Cu 2p regions of HfO_2: Cu thin films for different DC sputter power.

This was also evidenced in the core-level spectra of the Ag 3*d* and XRD peaks.

Fig. 10 (c) shows the deconvoluted Ag 3*d* spectra of HfO_2: Ag thin films. The Ag 3*d* peaks were fitted to two peaks located at 367.80 and 373.80 eV, which correspond to the spin-orbital splitting of Ag $3d_{5/2}$ and Ag $3d_{3/2}$, respectively. The binding energy peak positions and spin-orbital splitting energy values were constant for all DC sputtering power values (367.80 eV for Ag $3d_{5/2}$, 373.80 eV for Ag $3d_{3/2}$ and 5 eV, respectively). These binding energy values confirm the presence of Ag ions in Ag_2O (Ag^{+}) and/or AgO [70–72]. This oxidized state of Ag is also confirmed by the binding energy values (~530.50 eV) of non-lattice oxygen [70,72].

Similarly, deconvoluted core-level peaks of HfO_2: Cu thin films are observed in Fig. 11 (a). As mentioned, the spin-orbital splitting energy was constant (~1.61 eV) for all HfO_2: Cu samples. This indicates that Hf exists as Hf^{4+} and Hf–O bonding exists, and Cu doping does not change the chemical state of Hf [35,61–63]. In general, the electron configuration of metallic copper (Cu^0) consists of a filled 3*d* band and a partially filled Cu 4*s* band. In such a case, the binding energy of metallic copper is 932.5 eV [73–75]. In the case of Cu^{2+}, namely for CuO, this causes the Cu $2p_{3/2}$ peak to shift to a higher binding energy of 1.1 eV, resulting in the appearance of a weak satellite peak at 943 eV [73,76,77]. As can be seen in Fig. 11 (c), satellite peak is remarkably low and the Cu $2p_{3/2}$ binding energy shifted towards higher values. Also, Fig. 11 (c) shows the deconvoluted Cu 2*p* spectra of HfO_2: Cu thin films. Here, Cu $2p_{3/2}$ binding energies at a DC sputtering power at 5 W, 10 W and 20 W were 933.30 eV, 933.40 eV and 933.02 eV, respectively. So, the shift in Cu $2p_{3/2}$ binding energies to higher values and the absence of the satellite peak indicate the presence of Cu^{1+} phase in Cu_2O. Similarly to Ag, deconvoluted O 1*s* spectra of HfO_2: Cu thin films peaks at ~530 eV (O 1sA) also associated with the formation of Cu^{1+} [77].

Although no significant changes, due to the dopant atoms, were observed in the Hf environment, changes in the binding energies of both the dopant atoms and oxygen were observed. Doping HfO_2 films with metals increased the number of oxygen vacancies in the films. These oxygen-deficient dopant metal oxides significantly contribute to the conductivity of films and discussed in following section.

3.3. Electrical properties

3.3.1. Transfer length method

The transfer length method (TLM) was applied to Ag- and Cu-doped HfO_2 thin films. Unlike bulk materials, current flow occurs just below the surface in thin films, causing a current crowding phenomenon (Fig. 12). TLM considers this phenomenon and, in particular, enables the determination of thin films' DC characteristics (conductivity/resistivity) [78–80].

The following equation gives the total resistance (R_T) between the TLM patterns [79,80]:

$$R_T = \frac{2R_{SK}L_T}{w} + \frac{2R_{SH}l}{w} \tag{3}$$

where, w and l are the pad width and length, respectively, R_{SH}, R_{SK} modified sheet resistance outside the contact, and sheet resistance under the contact, respectively. R_T values are determined from the experimental I–V data (given in Table 4.). R_T versus gap spacing plots give a straight line and slope, and intercepts can be used to calculate the contact resistance (R_C) and transfer length (L_T), respectively (Fig. 13.). Also, under the condition $d \gg L_T$ and $R_T = 0$, the following equation can be written for the specific contact resistance (ρ_c) [80];

$$\rho_c = R_{SH}L_T^2. \tag{4}$$

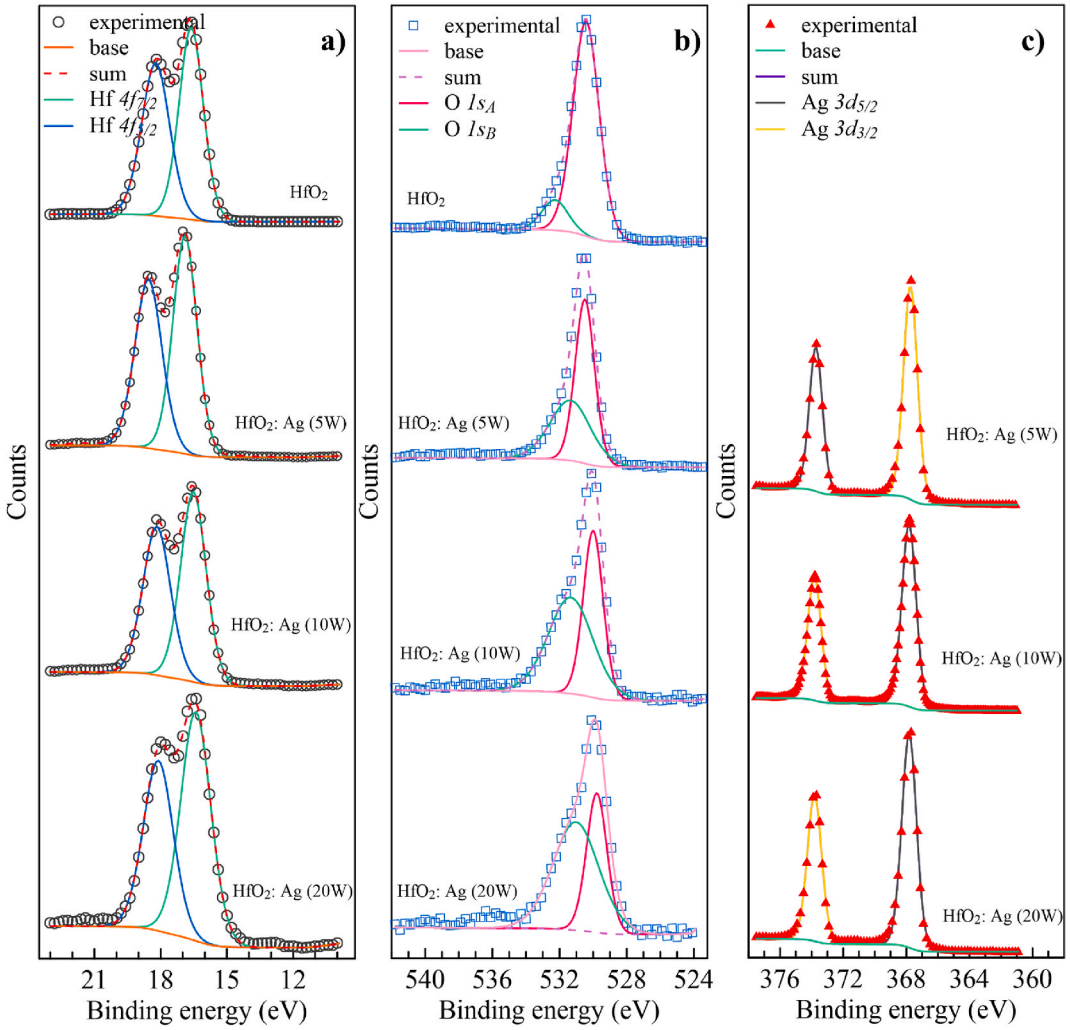

Fig. 10. Deconvoluted core-level spectra of the Hf 4*f* (a), O 1*s* (b), and Ag 3*d* (c) regions of HfO_2: Ag thin films prepared at different DC sputter powers.

Table 3
The calculated area ratio (at. %) of the O 1sA and O 1sB peaks.

Sample name	Ag-doped HfO_2		Cu-doped HfO_2	
	Lattice oxygen (O $1s_A$) (at. %)	Non-lattice oxygen (O $1s_B$) (at. %)	Lattice oxygen (O $1s_A$) (at. %)	Non-lattice oxygen (O $1s_B$) (at. %)
undoped	87.7	12.3	84.9	15.1
5 W	56.8	43.2	53.3	46.7
10 W	42.7	57.3	81.5	18.6
20 W	35.2	64.8	50.9	49.1

The specific contact resistivity, effective transfer length contact, and contact resistance of the undoped HfO_2 films was 1092.362 Ω□, 703.354 μm and 44.733x10^6 Ωcm^2, respectively. These values dramatically changed when the HfO_2 films were doped with silver (Table 4.). Silver ions significantly contribute to film conductivity by controlling the oxidation states of HfO_2 and affecting the non-lattice oxygen content (discussed later). As observed in the EDS results, increasing the DC sputtering power caused an increase in the dopant content; this dopant content change slightly increased the contact parameters. The dependency on the doping percentage of Ag can be explained by the influence of some morphological parameters and an increase in local tension due to the ionic radius of Ag^+ [81].

Similarly, copper doping caused a drop in contact parameter values, but these drops were limited compared to silver doping. In addition, contrary to the increase in contact parameters observed in the case of the silver doping ratio, the increase in doping ratio causes a decrease in contact parameters in copper-doped thin films.

These two contradictory behaviors observed in HfO_2 films deposited and doped using the same method can be explained by the different behaviors of Ag and Cu in the chemical structures of HfO_2 films. Many parameters, such as the number of valence electrons [82], electronegativity, work function, and Gibbs free energy of the alloys that may form, are effective for chemical changes such as oxygen vacancy, non-lattice oxygen, and oxidation of dopant atoms, which affect the conductivity of films. Also, as we know, the current conduction mechanism could raise the trap-assisted tunneling (due to the oxygen vacancy) [83–87] and/or donor (due to dopant atoms) related mechanism [18,88].

3.4. Electrochemical measurement

3.4.1. Potentiodynamic polarization evaluation

HfO_2 thin films have been investigated in electronic applications owing to their dielectric properties [89] and in corrosion research owing to their protective properties [90,91]. Many scientific studies use polarization tests and coated surface Tafel curves to elucidate electrochemical behavior [92–94]. Potentiodynamic polarization analyses investigated the potential corrosion of the deposited undoped HfO_2, Ag-doped, and Cu-doped HfO_2 thin films. Polarization measurements of the thin films were performed in 0.1 M KOH solution in the potential range −0.4 to +0.4 V at a scan rate of 1 mV/s. The experiments were

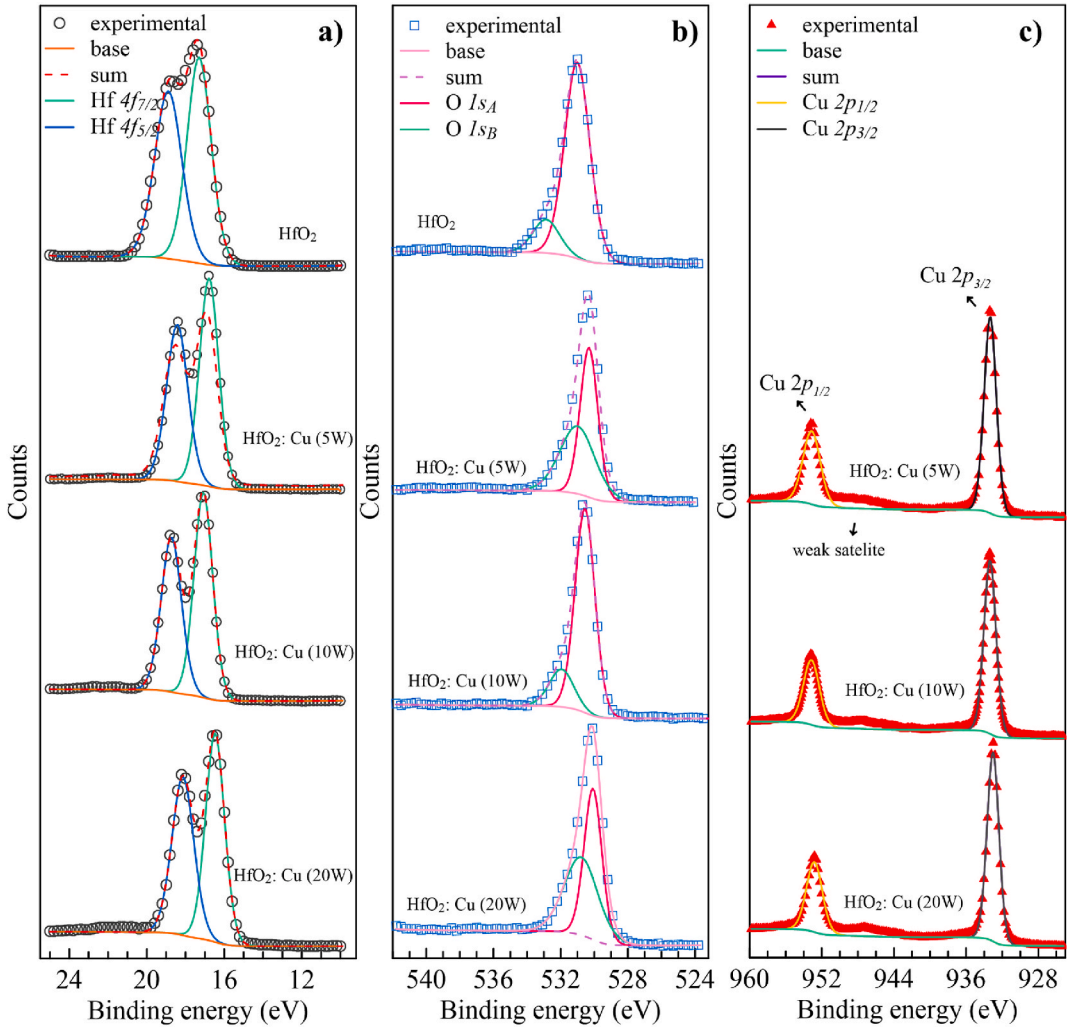

Fig. 11. Deconvoluted core-level spectra of the Hf 4*f* (a), O 1*s* (b), and Cu 2*p* (c) regions of HfO_2: Cu thin films for different DC sputter power.

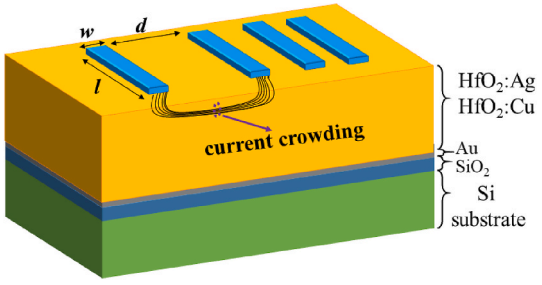

Fig. 12. Schematic representation of TLM patterns and current crowding in thin films. Four identical contacts at a certain distance from each other, and the total resistance (R_T) calculated from I–V measurements between them.

conducted in a three-electrode measurement system using thin film samples with an active surface area of 1 cm^2 as the working electrode, a Pt wire counter electrode, and an Ag/AgCl reference electrode. The Tafel curves are shown in Fig. 14. The corrosion potential (E_{corr}) of the HfO_2 thin film was −50 mV, and the corrosion potential shifted toward positive with the addition of Ag and toward more negative with the addition of Cu. A positive shift in the E_{corr} value (higher potential) is generally considered to indicate that the surface is more resistant to corrosion [95]. E_{corr} values indicate that the Ag-doped thin-film surface is more corrosion-resistant than HfO_2. On the contrary, upon the addition of Cu, the resistance of the HfO_2 thin film to corrosion attack decreased [96]. The more negative corrosion potential of the Cu-doped HfO_2 thin films compared to the Ag-doped thin films indicates that the Cu-doped HfO_2 films are more prone to corrosion. The larger grain boundaries observed in the FESEM surface images of Cu-doped HfO_2 films may provide an effective path for corrosion. The larger grain boundaries observed in the FESEM surface images of Cu-doped HfO_2 films may provide an effective

Table 4
Resistance measurements and TLM results of HfO_2: Ag and HfO_2: Cu thin films.

Sample name	Ag-doped HfO_2 (HfO_2: Ag)			Cu-doped HfO_2 (HfO_2: Ag)		
	L_T (μm)	ρ_c (Ω□)	R_c (Ωcm^2)	L_T (μm)	ρ_c (Ω□)	R_c (Ωcm^2)
undoped	–	–	–	703.354	1092.362	44.733x10^6
5 W	8.582	8.945x10^{-5}	4.427	33.727	203.499	8.425x10^6
10 W	28.521	1.151x10^{-4}	4.792	38.490	208.004	8.583x10^6
20 W	94.101	1.229x10^{-4}	5.025	11.058	118.475	5.465x10^6

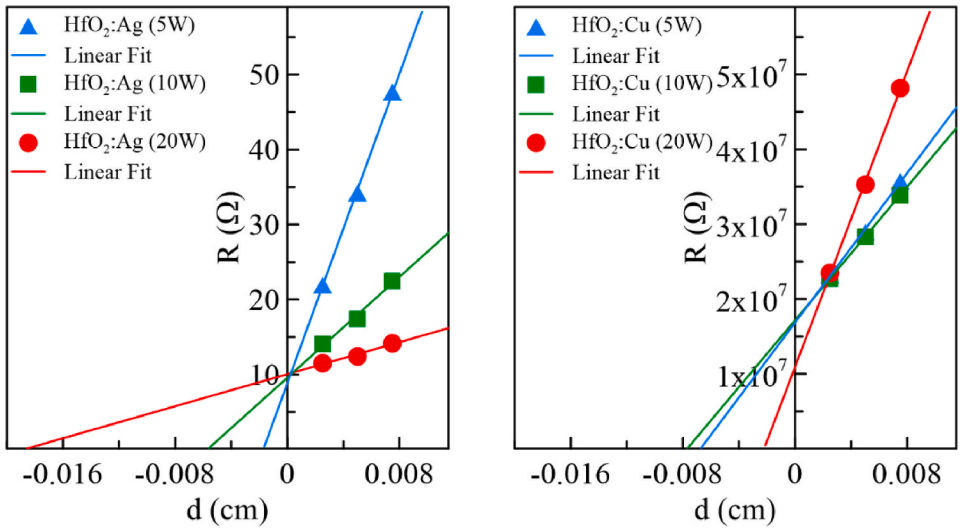

Fig. 13. R_T versus gap-spacing (d) plots of HfO_2: Ag and HfO_2: Cu thin films.

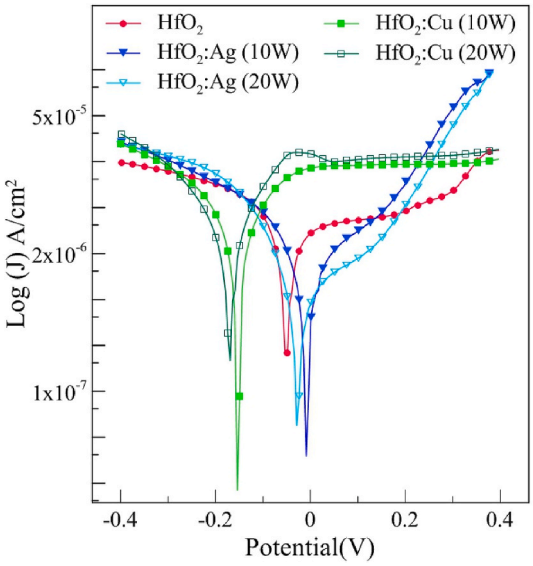

Fig. 14. Tafel plots of Ag-doped HfO_2 and Cu-doped HfO_2 thin film samples.

path for corrosion. These results regarding the effects of grain boundaries on corrosion were also consistent with the literature [97].

Corrosion current density (J_{corr}) values of the samples are important parameters for evaluating corrosion behavior. Moreover, polarization resistance (R_p) is an essential parameter for detecting and evaluating the anti-corrosion behavior of the protective layer on the sample surface. R_p value was calculated using the help of Equation (5) [98] below;

$$R_p = \frac{\beta_a \times \beta_c}{(\beta_a + \beta_c) \times 2.3 \times J_{corr}} \quad (5)$$

where β_a and β_c are the slopes of the anodic and cathodic sides obtained from the Tafel plots, respectively. J_{corr} and R_p values of the thin films are shown in Fig. 15. By comparing the J_{corr} values, it can be seen that the value tends to decrease with Ag doping and increases with Cu doping compared to the HfO_2 sample. Cu-doped HfO_2 films, which are prone to corrosion as seen with their corrosion potential also have a higher corrosion rate, as further evidenced by corrosion current density values. The highest J_{corr} value of 5.28 μA/cm^2 was obtained for the HfO_2: Cu (20 W) sample, whereas the lowest value of 0.92 μA/cm^2 was obtained

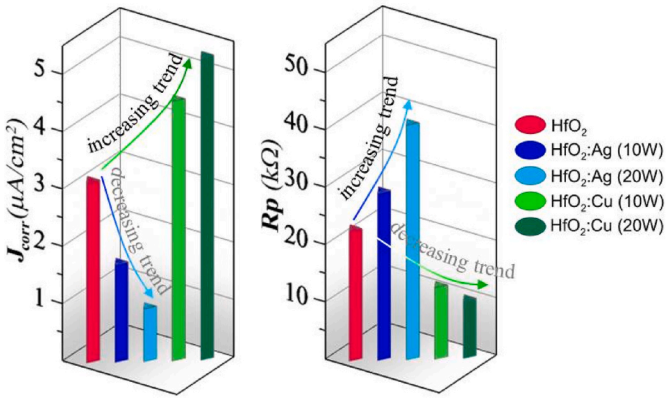

Fig. 15. J_{corr} and R_p values of doped and undoped HfO_2 thin films were obtained from Tafel plots.

for the HfO_2: Ag (20 W) sample. Thus, Ag doping to HfO_2 can increase the protection against corrosion attacks, whereas Cu doping can reduce this protection. A comparison of R_p values shows that R_p tends to increase with Ag doping and decreases with Cu doping, which supports the current density results. The highest and lowest R_p values were obtained as 40.91 kΩ for HfO_2: Ag (20 W) thin film and 10.03 kΩ for HfO_2: Cu (20 W), respectively.

The electrochemical parameters of the thin-film samples were obtained from Tafel analysis using IVMAN™ Main Software (WonATech Co., Ltd.) and are summarized in Table 5. In addition, porosity can be considered a parameter that should be considered in corrosion behavior. The porosity of the thin-film coatings was estimated using the following empirical formula [99] given in Equation (6) below;

$$\text{Porosity} = \frac{R_{p\ (substrate)}}{R_{p\ (thin\ film)}} \times 10^{\left\{\frac{-|\Delta E_{corr}|}{\beta_{a\ (substrate)}}\right\}} \quad (6)$$

here, ΔE_{corr} is the difference in corrosion potentials obtained from the Tafel plot. β_a value is the slope of the anodic side in the Tafel plot for bare SiO_2 used as the substrate. It was obtained as 297 mV. The results show that the porosity increased from 0.79 to 0.89 (for 20 W) with Cu addition, and the increase in particle size may have increased the porosity, thus resulting in a more porous, thin film and decreased corrosion resistance.

In the literature, it was reported by Mahendra, N. et al. [100] based

Table 5
Calculated potentiodynamic polarization parameters.

Sample name	E_{corr} (mV)	$\lvert\Delta E_{corr}\rvert$ (mV)	J_{corr} (μA/cm^2)	β_a (mV)	$-\beta_c$ (mV)	R_p (kΩ)	Porosity
HfO_2	−50.00	15.30	3.15	694	216	22.75	0.79
HfO_2: Ag (10 W)	−9.20	56.10	1.71	326	177	29.22	0.45
HfO_2: Ag (20 W)	−26.80	38.50	0.92	366	114	40.91	0.37
HfO_2: Cu (10 W)	−154.23	88.93	4.53	256	265	12.49	0.81
HfO_2: Cu (20 W)	−170.35	105.05	5.28	217	277	10.03	0.89

on HR-TEM analysis, that Cu doping with HfO_2 increases particle size. The results of our study also support this electrochemical situation. In addition, the XRD analysis also supported the porosity results. As a result, polarization analyses showed that adding Cu to the HfO_2 thin film reduced the corrosion resistance in alkaline environments, whereas adding Ag increased the corrosion resistance. This may be due to morphological and structural changes in the thin-film structure (such as porosity, grain formation and size) or the electrochemical behavior of the dopant elements. In addition, the higher presence of non-lattice oxygen detected from the XPS peaks of Ag-doped samples may provide passivation of HfO_2: Ag films in solution and thus reduced their electrochemical activity.

In summary, this study investigated the structural, electrical, and electrochemical properties of Cu- and Ag-doped HfO_2 thin films deposited via co-sputtering. The findings revealed that the dopant concentration, controlled by varying the DC magnetron sputtering power, significantly influenced the surface morphology, crystalline structure, and electrical behavior of the films. AFM and FE-SEM analyses demonstrated that Ag doping led to relatively smooth and uniform films, while Cu doping resulted in more irregular and rougher morphologies, particularly at higher sputtering powers. XPS analysis confirmed the successful incorporation of dopants, with Ag causing a slight shift in the spin-orbit splitting of Hf, whereas Cu did not induce significant changes. Electrical measurements indicated an increase in conductivity for both dopants, albeit with distinct underlying mechanisms. Additionally, potentiodynamic polarization analysis demonstrated that Ag doping improved corrosion resistance, while Cu doping reduced it. These results provide a comprehensive understanding of the impact of Cu and Ag doping on HfO_2 films, paving the way for optimized applications in electronic and electrochemical devices.

4. Conclusion

The study of HfO_2: Ag and HfO_2: Cu thin films deposited via co-sputtering has provided significant insights into their structural, electrical, and electrochemical properties. Precise control of dopant concentration through varying DC magnetron sputtering power enabled a systematic evaluation of their impact on film characteristics.

Experimental findings highlight the crucial role of dopant type and sputtering power in determining film properties. AFM and FE-SEM analyses indicated that increasing Ag content initially led to island-type (Volmer-Weber) growth, transitioning to a more uniform structure at higher power levels, whereas Cu-doped films exhibited increased roughness, signifying a dominant island type growth mechanism. Ag doping improved surface smoothness, while Cu doping resulted in a more irregular and brittle structure. XRD results confirmed that the primary HfO_2 phase remained monoclinic, with Ag and Cu doping inducing minor structural modifications without major phase transitions. Increased doping enhanced crystallinity, leading to a transition from an amorphous to a predominantly small-crystalline phase. XPS analysis verified dopant incorporation, showing Ag influenced spin-orbit splitting and non-lattice oxygen content, while Cu affected oxidation states without significantly altering the Hf environment.

Electrical characterization using the transfer length method (TLM) demonstrated enhanced conductivity for both doped films. Silver doping significantly increased contact parameters by influencing oxidation states and non-lattice oxygen content, whereas copper doping reduced them. The nonlinear relationship between conductivity and dopant concentration suggested complex charge transport mechanisms driven by oxidation states and film morphology. Electrochemical analysis showed that Ag doping improved corrosion resistance, while Cu doping decreased it due to differences in film porosity and oxidation states. These findings underscore the tunability of HfO_2 thin films for applications like resistive switching memory, gate dielectrics, and corrosion-resistant coatings.

Overall, this study demonstrates the effectiveness of co-sputtering in tailoring HfO_2 thin film properties through controlled doping. The insights gained contribute to the broader understanding of metal-doped oxides, potentially guiding the development of next-generation electronic and electrochemical devices. Future research may focus on optimizing deposition parameters and post-deposition treatments to further enhance film performance and stability.

CRediT authorship contribution statement

Abdullah Akkaya: Writing – review & editing, Writing – original draft, Software, Investigation, Formal analysis, Data curation, Conceptualization. **Osman Kahveci:** Writing – review & editing, Writing – original draft, Software, Data curation, Conceptualization. **Sedanur Güler:** Visualization, Investigation. **Enise Ayyıldız:** Supervision, Project administration, Funding acquisition, Conceptualization.

Declaration of competing interest

The authors declare the following financial interests/personal relationships which may be considered as potential competing interests: Enise Ayyildiz reports financial support was provided by Erciyes University Scientific Research Projects Coordination Unit (BAP). If there are other authors, they declare that they have no known competing financial interests or personal relationships that could have appeared to influence the work reported in this paper.

Acknowledgments

This work was supported by the Erciyes University Scientific Research Projects Coordination Unit (BAP, grant number FYL-2023-12720). The authors gratefully acknowledge financial support from BAP. We would like to also thank the Proofreading & Editing Office of the Dean for Research at Erciyes University, for the copyediting and proofreading services for this manuscript.

Data availability

Data will be made available on request.

References

[1] J.H. Choi, Y. Mao, J.P. Chang, Development of hafnium based high-k materials—a review, Materials Science and Engineering: r, Report 72 (2011) 97–136.
[2] G.D. Wilk, R.M. Wallace, J.M. Anthony, High-κ gate dielectrics: current status and materials properties considerations, J. Appl. Phys. 89 (2001) 5243–5275.

[3] J. Liao, S. Dai, R.-C. Peng, J. Yang, B. Zeng, M. Liao, Y. Zhou, HfO_2-based ferroelectric thin film and memory device applications in the post-Moore era: a review, Fundamental Research 3 (2023) 332–345.

[4] J. Robertson, High dielectric constant oxides, Eur. Phys. J. Appl. Phys. 28 (2004) 265–291.

[5] M. Liu, L.D. Zhang, G. He, X.J. Wang, M. Fang, Effect of Ti incorporation on the interfacial and optical properties of HfTiO thin films, J. Appl. Phys. 108 (2010).

[6] Y. Zhang, J. Xu, D.-Y. Zhou, H.-H. Wang, W.-Q. Lu, C.-K. Choi, Structural and electrical properties of reactive magnetron sputtered yttrium-doped HfO_2 films, Chin. Phys. B 27 (2018) 048103.

[7] J.M. Khoshman, M.E. Kordesch, Optical properties of a-HfO_2 thin films, Surf. Coating. Technol. 201 (2006) 3530–3535.

[8] P. Chen, N. Ilyas, C. Li, D. Li, X. Jiang, W. Li, Memristive behaviour of Ag-doped-HfO2 thin films prepared by magnetron sputtering, J. Phys. Conf. 1637 (2020) 012024.

[9] S. Lee, W.G. Kim, S.W. Rhee, K. Yong, Resistance switching behaviors of hafnium oxide films grown by MOCVD for nonvolatile memory applications, J. Electrochem. Soc. 155 (2008) H92–H96.

[10] R. Zhang, Y. Ma, Y. Tang, D. Goonetilleke, T. Diemant, J. Janek, A. Kondrakov, T. Brezesinski, Conformal Li_2HfO_3/HfO_2 nanoparticle coatings on layered Ni-rich oxide cathodes for stabilizing interfaces in all-solid-state batteries, Chem. Mater. 35 (2023) 6835–6844.

[11] M. Mäntymäki, E. Atosuo, M.J. Heikkilä, M. Vehkamäki, M. Mattinen, K. Mizohata, J. Räisänen, M. Ritala, M. Leskelä, Studies on solid state reactions of atomic layer deposited thin films of lithium carbonate with hafnia and zirconia, J. Vac. Sci. Technol. A (2019) 37.

[12] S. Zhuiykov, An investigation of conductivity, microstructure and stability of HfO_2–ZrO_2–Y_2O_3–Al_2O_3 electrolyte compositions for high-temperature oxygen measurement, J. Eur. Ceram. Soc. 20 (2000) 967–976.

[13] H.A. Hsain, Y. Lee, M. Materano, T. Mittmann, A. Payne, T. Mikolajick, U. Schroeder, G.N. Parsons, J.L. Jones, Many routes to ferroelectric HfO_2: a review of current deposition methods, J. Vac. Sci. Technol. A 40 (2022) 010803.

[14] V. Dave, P. Dubey, H.O. Gupta, R. Chandra, Effect of sputtering gas on structural, optical and hydrophobic properties of DC-sputtered hafnium oxide thin films, Surf. Coating. Technol. 232 (2013) 425–431.

[15] D. Triyoso, R. Liu, D. Roan, M. Ramon, N.V. Edwards, R. Gregory, D. Werho, J. Kulik, G. Tam, E. Irwin, X.D. Wang, L.B. La, C. Hobbs, R. Garcia, J. Baker, B. E. White, P. Tobin, Impact of deposition and annealing temperature on material and electrical characteristics of ALD HfO_2, J. Electrochem. Soc. 151 (2004) F220.

[16] K. Beckmann, N. Suguitan, J. Van Nostrand, N.C. Cady, Interface modification of HfO_2-based ReRAM via low temperature anneal, Semicond. Sci. Technol. 34 (2019) 105021.

[17] G. He, M. Liu, L.Q. Zhu, M. Chang, Q. Fang, L.D. Zhang, Effect of postdeposition annealing on the thermal stability and structural characteristics of sputtered HfO_2 films on Si (100), Surf. Sci. 576 (2005) 67–75.

[18] A. Akkaya, O. Kahveci, B. Şahin, E. Ayyıldız, Simultaneously-doping of HfO_2 thin films by Ni with sputtering technique and effect of post annealing on structural and electrical properties, Phys. B Condens. Matter 665 (2023) 415034.

[19] J. Ho Lee, I.-H. Yu, S. Young Lee, C. Seong Hwang, Phase control of HfO_2-based dielectric films for higher-k materials, J. Vac. Sci. Technol. B (2014) 32.

[20] J.d.J. Araiza, L. Álvarez-Fraga, R. Gago, O. Sánchez, Surface morphology and optical properties of hafnium oxide thin films produced by magnetron sputtering, Materials 16 (2023) 5331.

[21] O. Pakma, S. Kaval, İ.A. Kariper, Ag-doped HfO_2 thin films via sol–gel dip coating method, Opt. Quant. Electron. 51 (2019) 342.

[22] T. Torchynska, L. Vega Macotela, L. Khomenkova, F. Gourbilleau, L. Lartundo Rojas, Annealing impact on emission and phase varying of Nd-doped Si-rich-HfO_2 films prepared by RF magnetron sputtering, J. Mater. Sci. Mater. Electron. 31 (2020) 4587–4594.

[23] S.-S. Lin, C.-S. Liao, Structure and physical properties of W-doped HfO_2 thin films deposited by simultaneous RF and DC magnetron sputtering, Surf. Coating. Technol. 232 (2013) 46–52.

[24] M. Akbari, J.-S. Lee, Control of resistive switching behaviors of solution-processed HfO_X-based resistive switching memory devices by n-type doping, RSC Adv. 6 (2016) 21917–21921.

[25] M.H. Park, T. Schenk, C.M. Fancher, E.D. Grimley, C. Zhou, C. Richter, J. M. LeBeau, J.L. Jones, T. Mikolajick, U. Schroeder, A comprehensive study on the structural evolution of HfO_2 thin films doped with various dopants, J. Mater. Chem. C 5 (2017) 4677–4690.

[26] S. Gálvez-Barboza, L.A. García-Cerda, L.A. González, Effect of Ce doping on the structure and optical properties of HfO_2 films by the Pechini-type sol–gel method, J. Sol. Gel Sci. Technol. 88 (2018) 371–378.

[27] M. Esplandiu, L. Avalle, V. Macagno, Characterization of hafnium oxide films modified by Pt doping, Electrochim. Acta 40 (1995) 2587–2593.

[28] V. Mantella, L. Castilla-Amorós, R. Buonsanti, Shaping non-noble metal nanocrystals via colloidal chemistry, Chem. Sci. 11 (2020) 11394–11403.

[29] M. Alqadi, A. Migdadi, F. Alzoubi, H. Al-Khateeb, A.A. Almasri, Influence of (Ag–Cu) co-doping on the optical, structural, electrical, and morphological properties of ZnO thin films, J. Sol. Gel Sci. Technol. 103 (2022) 319–334.

[30] K.O. Egbo, C.E. Ekuma, C.P. Liu, K.M. Yu, Efficient *p*-type doping of sputter-deposited NiO thin films with Li, Ag, and Cu acceptors, Phys. Rev. Mater. 4 (2020) 104603.

[31] W. Zhao, Y. Fang, W. Li, X. Han, Impact of Ag doping on Cu_3BiS_3 solar cell performance, Sol. Energy 221 (2021) 109–113.

[32] S. Ballikaya, H. Chi, J.R. Salvador, C. Uher, Thermoelectric properties of Ag-doped Cu_2Se and Cu_2Te, J. Mater. Chem. A 1 (2013) 12478–12484.

[33] C. Li, Y. Ma, Z. Xue, Y. Yang, J. Chen, H. Guo, Effect of Y doping on microstructure and thermophysical properties of yttria stabilized hafnia ceramics, Ceram. Int. 44 (2018) 18213–18221.

[34] X. Cui, K. Tuokedaerhan, H. Cai, Z. Lu, Effect of annealing temperature on the microstructure and optical properties of lanthanum-doped hafnium oxide, Coatings 12 (2022) 439.

[35] M. Kumar Sharma, D. Kumar Mishra, S. Ghosh, D. Kanjilal, P. Srivastava, R. Chatterjee, Oxygen vacancy mediated large magnetization in chemically synthesized Ni-doped HfO_2 nanoparticle powder samples, J. Appl. Phys. 110 (2011).

[36] C.-W. Wu, C.-C. Lin, P.-H. Chen, T.-C. Chang, K.-J. Zhou, W.-C. Chen, Y.-F. Tan, Y.-H. Yeh, S.-Y. Chou, H.-C. Huang, T.-M. Tsai, S.M. Sze, Realizing forming-free characteristic by doping Ag into HfO2-based RRAM, Appl Phys Express 14 (2021) 041008.

[37] W. Kern, Handbook of Semiconductor Wafer Cleaning Technology, Noyes Park Ridge, Westwood New Jersey, 1993.

[38] A. Akkaya, E. Ayyıldız, Automation software for semiconductor research laboratories: electrical parameter calculation program (SeCLaS-PC), J. Circ. Syst. Comput. 29 (2020) 2050215.

[39] A. Akkaya, E. Ayyıldız, Automation software for semiconductor research laboratories: measurement system and instrument control program (SeCLaS-IC), MAPAN 35 (2020) 343–350.

[40] M. Haemori, T. Nagata, T. Chikyow, Impact of Cu electrode on switching behavior in a Cu/HfO_2/Pt structure and resultant Cu ion diffusion, Appl Phys Express 2 (2009) 061401.

[41] H.J. Park, Y.M. Sun, H. Troiani, P. Santiago, M.J. Yacaman, J.M. White, Growth and thermal annealing of Cu on HfO_2, Surf. Sci. 521 (2002) 1–9.

[42] A.G. Khairnar, A.M. Mahajan, Effect of post-deposition annealing temperature on RF-sputtered HfO_2 thin film for advanced CMOS technology, Solid State Sci. 15 (2013) 24–28.

[43] R.K. Jain, Y.K. Gautam, V. Dave, A.K. Chawla, R. Chandra, A study on structural, optical and hydrophobic properties of oblique angle sputter deposited HfO_2 films, Appl. Surf. Sci. 283 (2013) 332–338.

[44] C.V. Ramana, K.K. Bharathi, A. Garcia, A.L. Campbell, Growth behavior, lattice expansion, strain, and surface morphology of nanocrystalline, monoclinic HfO_2 thin films, J. Phys. Chem. C 116 (2012) 9955–9960.

[45] R.W. Vook, Structure and growth of thin films, Int. Met. Rev. 27 (1982) 209–245.

[46] S. Ghosh, H. Kim, K. Hong, C. Lee, Microstructure of indium tin oxide films deposited on porous silicon by rf-sputtering, Mater. Sci. Eng., B 95 (2002) 171–179.

[47] U. Schroeder, M.H. Park, T. Mikolajick, C.S. Hwang, The fundamentals and applications of ferroelectric HfO_2, Nat. Rev. Mater. 7 (2022) 653–669.

[48] E. Stevens, Y. Tomczak, B.T. Chan, E. Altamirano Sanchez, G.N. Parsons, A. Delabie, Area-Selective atomic layer deposition of TiN, TiO_2, and HfO_2 on silicon nitride with inhibition on amorphous carbon, Chem. Mater. 30 (2018) 3223–3232.

[49] A. Chaoumead, Y.-m. Sung, D.-J. Kwak, The effects of RF sputtering power and gas pressure on structural and electrical properties of ITiO thin film, Adv. Condens. Matter Phys. 2012 (2012) 651587.

[50] H. Adachi, T. Hata, K. Wasa, Basic process of sputtering deposition, in: K. Wasa (Ed.), Handbook of Sputter Deposition Technology: Fundamentals and Applications for Functional Thin Films, Nano-Materials and MEMS, William Andrew, Waltham, 2012, p. 295.

[51] L. Khomenkova, X. Portier, P. Marie, F. Gourbilleau, Hafnium silicate dielectrics fabricated by RF magnetron sputtering, J. Non-Cryst. Solids 357 (2011) 1860–1865.

[52] A. Cantas, G. Aygun, D.K. Basa, In-situ spectroscopic ellipsometry and structural study of HfO_2 thin films deposited by radio frequency magnetron sputtering, J. Appl. Phys. 116 (2014).

[53] H. Hahn, R.S. Averback, The production of nanocrystalline powders by magnetron sputtering, J. Appl. Phys. 67 (1990) 1113–1115.

[54] N. Selvakumar, H.C. Barshilia, K.S. Rajam, A. Biswas, Structure, optical properties and thermal stability of pulsed sputter deposited high temperature HfO_x/Mo/HfO_2 solar selective absorbers, Sol. Energy Mater. Sol. Cell. 94 (2010) 1412–1420.

[55] S. Chen, Z. Liu, L. Feng, X. Che, X. Zhao, Effect of ytterbium inclusion in hafnium oxide on the structural and electrical properties of the high-k gate dielectric, J. Rare Earths 32 (2014) 580–584.

[56] P.M. Tirmali, A.G. Khairnar, B.N. Joshi, A.M. Mahajan, Structural and electrical characteristics of RF-sputtered HfO_2 high-k based MOS capacitors, Solid State Electron. 62 (2011) 44–47.

[57] T. Tan, Z. Liu, H. Lu, W. Liu, H. Tian, Structure and optical properties of HfO_2 thin films on silicon after rapid thermal annealing, Opt. Mater. 32 (2010) 432–435.

[58] T.P. Smirnova, L.V. Yakovkina, V.O. Borisov, M.S. Lebedev, Phase composition of nanosized oxide film structures based on lanthanum and scandium doped HfO_2, J. Struct. Chem. 58 (2017) 1573–1580.

[59] K.-Y. Chan, B.-S. Teo, Atomic force microscopy (AFM) and X-ray diffraction (XRD) investigations of copper thin films prepared by dc magnetron sputtering technique, Microelectron. J. 37 (2006) 1064–1071.

[60] Y. Igasaki, H. Kanma, Argon gas pressure dependence of the properties of transparent conducting ZnO:Al films deposited on glass substrates, Appl. Surf. Sci. 169–170 (2001) 508–511.

[61] K.C. Das, S.P. Ghosh, N. Tripathy, D. Pradhan, R. Singhal, A. Nakamura, J.P. Kar, Role of Gd dopants on electrical properties of RF co-sputtered HfO2 thin films for resistive switching applications, Mater. Sci. Eng., B 265 (2021) 114997.

[62] M. Engelhard, J. Herman, R. Wallace, D. Baer, As-received, ozone cleaned and Ar^+ sputtered surfaces of hafnium oxide grown by atomic layer deposition and studied by XPS, Surf. Sci. Spectra 18 (2011) 46–57.
[63] J.-H. Hong, T.-H. Moon, J.-M. Myoung, Microstructure and characteristics of the HfO_2 dielectric layers grown by metalorganic molecular beam epitaxy, Microelectron. Eng. 75 (2004) 263–268.
[64] P.S. Bagus, F. Illas, G. Pacchioni, F. Parmigiani, Mechanisms responsible for chemical shifts of core-level binding energies and their relationship to chemical bonding, J Electron. Spectrosc. 100 (1999) 215–236.
[65] M.J. Guittet, J.P. Crocombette, M. Gautier-Soyer, Bonding and XPS chemical shifts in $ZrSiO_4$ versus SiO_2 and ZrO_2 : charge transfer and electrostatic effects, Phys. Rev. B 63 (2001) 125117.
[66] T. Guo, T. Tan, Z. Liu, B. Liu, Oxygen vacancy modulation and enhanced switching behavior in HfO_x film induced by Al doping effect, J. Alloys Compd. 686 (2016) 669–674.
[67] G. Greczynski, L. Hultman, X-ray photoelectron spectroscopy: towards reliable binding energy referencing, Prog. Mater. Sci. 107 (2020) 100591.
[68] S.H. Abud, A. Ramiy, A.S. Hussein, Z. Hassan, F.K. Yam, A comparative study of the structural and electrical properties of n-type InGaN epilayer grown by MBE and commercially, Superlattice. Microst. 60 (2013) 224–230.
[69] A. Vinod, M.S. Rathore, N. Srinivasa Rao, Effects of annealing on quality and stoichiometry of HfO_2 thin films grown by RF magnetron sputtering, Vacuum 155 (2018) 339–344.
[70] A.I. Boronin, S.V. Koscheev, G.M. Zhidomirov, XPS and UPS study of oxygen states on silver, J Electron. Spectrosc. 96 (1998) 43–51.
[71] P. Prieto, V. Nistor, K. Nouneh, M. Oyama, M. Abd-Lefdil, R. Díaz, XPS study of silver, nickel and bimetallic silver–nickel nanoparticles prepared by seed-mediated growth, Appl. Surf. Sci. 258 (2012) 8807–8813.
[72] V.K. Kaushik, XPS core level spectra and Auger parameters for some silver compounds, J Electron. Spectrosc. 56 (1991) 273–277.
[73] C. Zhu, A. Osherov, M.J. Panzer, Surface chemistry of electrodeposited Cu_2O films studied by XPS, Electrochim. Acta 111 (2013) 771–778.
[74] S. Poulston, P.M. Parlett, P. Stone, M. Bowker, Surface oxidation and reduction of CuO and Cu_2O studied using XPS and XAES, Surf. Interface Anal. 24 (1996) 811–820.
[75] T.M. Ivanova, K.I. Maslakov, A.A. Sidorov, M.A. Kiskin, R.V. Linko, S.V. Savilov, V.V. Lunin, I.L. Eremenko, XPS detection of unusual Cu(II) to Cu(I) transition on the surface of complexes with redox-active ligands, J Electron. Spectrosc. 238 (2020) 146878.
[76] N.-E. Sung, I.-J. Lee, A. Thakur, K.H. Chae, H.-J. Shin, H.-K. Lee, Properties of Cu-doped ZnO films by RF sputtering method: thickness dependence, Mater. Res. Bull. 47 (2012) 2891–2894.
[77] J.A. Torres-Ochoa, D. Cabrera-German, O. Cortazar-Martinez, M. Bravo-Sanchez, G. Gomez-Sosa, A. Herrera-Gomez, Peak-fitting of Cu 2p photoemission spectra in Cu^0, Cu^{1+}, and Cu^{2+} oxides: a method for discriminating Cu^0 from Cu^{1+}, Appl. Surf. Sci. 622 (2023) 156960.
[78] A. Akkaya, E. Ayyıldız, Depth profile study on Ti/Al bilayer Ohmic contacts to AlGaN/GaN, Mater. Today Proc. 46 (2021) 6939–6946.
[79] G.K. Reeves, H.B. Harrison, Obtaining the specific contact resistance from transmission-line model measurements, IEEE Electron Device Lett. 3 (1982) 111–113.
[80] D.K. Schroder, Semiconductor Material and Device Characterization, John Wiley & Sons, New York, 2006.
[81] O. Kahveci, A. Akkaya, R. Aydın, B. Şahin, E. Ayyıldız, Synthesis of Al and in dual-doped CuO nanostructures via SILAR method: structural, optical and electrical properties, Inorg. Chem. Commun. 147 (2023) 110230.
[82] W.J. Zhao Yuanyang, Xu Jianbin, Fei Yang, Qi Liu, Dai Yuehua, Metal dopants in HfO2-based RRAM: first principle study, J. Semiconduct. 35 (2014) 042002.
[83] J. Gao, G. He, J.W. Zhang, B. Deng, Y.M. Liu, Annealing temperature modulated interfacial chemistry and electrical characteristics of sputtering-derived HfO_2/Si gate stack, J. Alloys Compd. 647 (2015) 322–330.
[84] F. Gao, S.J. Lee, D.Z. Chi, S. Balakumar, D.-L. Kwong, GaAs metal-oxide-semiconductor device with HfO_2/TaN gate stack and thermal nitridation surface passivation, Appl. Phys. Lett. 90 (2007) 252904.
[85] M. Wen, J. Xu, L. Liu, P.-T. Lai, W.-M. Tang, Effects of annealing on electrical performance of multilayer MoS_2 transistors with atomic layer deposited HfO_2 gate dielectric, Appl Phys Express 9 (2016) 095202.
[86] S. Mohanty, I. Sayed, Z. Jian, U. Mishra, E. Ahmadi, Investigation and optimization of HfO_2 gate dielectric on N-polar GaN: impact of surface treatments, deposition, and annealing conditions, Appl. Phys. Lett. 119 (2021) 042901.
[87] P. Zhao, A. Azcatl, P. Bolshakov, J. Moon, C.L. Hinkle, P.K. Hurley, R.M. Wallace, C.D. Young, Effects of annealing on top-gated MoS_2 transistors with HfO_2 dielectric, J. Vac. Sci. Technol. B 35 (2017) 01A118.
[88] M.J. Iqbal, N. Yaqub, B. Sepiol, B. Ismail, A study of the influence of crystallite size on the electrical and magnetic properties of $CuFe_2O_4$, Mater. Res. Bull. 46 (2011) 1837–1842.
[89] F. Yan, J. Liao, K. Cao, S. Jia, Y. Zhou, M. Liao, Achieving excellent ferroelectric and dielectric performance of $HfO_2/ZrO_2/HfO_2$ thin films under low operating voltage, J. Alloys Compd. 968 (2023) 172267.
[90] E. Mańkowska, M. Mazur, M. Kalisz, M. Grobelny, J. Domaradzki, D. Wojcieszak, Characterization of structural, optical, corrosion, and mechanical properties of HfO_2 thin films deposited using pulsed DC magnetron sputtering, Materials 16 (2023) 5005.
[91] I. Spajić, P. Rodič, G. Šekularac, M. Lekka, L. Fedrizzi, I. Milošev, The effect of surface preparation on the protective properties of Al_2O_3 and HfO_2 thin films deposited on cp-titanium by atomic layer deposition, Electrochim. Acta 366 (2021) 137431.
[92] A.K. Gupta, N. Mandal, S. Nayak, R.S. Moirangthem, S.R.M. Reddy, A.N. Bhagat, T.K. Rout, Efficient and cost-effective single-step thin overlay zinc oxide nanostructure for enhanced corrosion protection of galvanized steel, Met. Mater. Int. (2024) 1–11.
[93] B. Hüner, N. Demir, M. Fatih Kaya, Fabrication and characterization of Nickel-coated 3D printed electrodes for enhanced oxygen evolution reaction in acidic media at various temperatures, Fuel 366 (2024) 131172.
[94] H.-J. Chen, Y.-C. Chen, P.-C. Lin, K. Lin, J.C. Lin, M.-J. Chen, H.-C. Lin, Study of atomic layer deposition nano-oxide films on corrosion protection of Al-SiC composites, Materials 16 (2023) 6149.
[95] M. Dinu, K. Wang, E.S.M. Mouele, A.C. Parau, A. Vladescu, X. Liang, V. Braic, L. F. Petrik, M. Braic, Effects of film thickness of ALD-deposited Al_2O_3, ZrO_2 and HfO_2 nano-layers on the corrosion resistance of Ti(N,O)-Coated stainless steel, Materials 16 (2023) 2007.
[96] M. Li, Z.-X. Jin, W. Zhang, Y.-H. Bai, Y.-Q. Cao, W.-M. Li, D. Wu, A.-D. Li, Comparison of chemical stability and corrosion resistance of group IV metal oxide films formed by thermal and plasma-enhanced atomic layer deposition, Sci Rep-Uk 9 (2019) 10438.
[97] A. Obeydavi, A. Shafyei, J.-W. Lee, Effect of sputtering power and substrate bias on microstructure, mechanical properties and corrosion behavior of CoCrFeMnNi high entropy alloy thin films deposited by magnetron sputtering method, Intermetallics 172 (2024) 108369.
[98] O. Kahveci, Preparation of 3-D porous pure Al electrode for Al-air battery anode and comparison of its electrochemical performance with a smooth surface electrode, Chemelectrochem 10 (2023) e202300221.
[99] I. Pana, V. Braic, M. Dinu, E.S.M. Mouele, A.C. Parau, L.F. Petrik, M. Braic, In vitro corrosion of titanium nitride and oxynitride-based biocompatible coatings deposited on stainless steel, Coatings 10 (2020) 710.
[100] N. Mahendran, S. Johnson Jeyakumar, M. Jothibas, M. Ponnar, A. Muthuvel, Synthesis, characterization of undoped and copper-doped hafnium oxide nanoparticles by sol–gel method, J. Mater. Sci. Mater. Electron. 33 (2022) 10439–10449.